Quantifying burning efficiency in Megacities using NO_2/CO ratio from the Tropospheric Monitoring Instrument (TROPOMI)

Srijana Lama[1], Sander Houweling[1,2], K. Folkert Boersma[3,4], Henk Eskes[4], Ilse Aben[2,5], Hugo A C Denier van der Gon[6], Maarten C. Krol[3,7], A.J.(Han) Dolman[1], Tobias Borsdorff [2], Alba Lorente[2]

[1]Vrije Universiteit, Department of Earth Sciences, Amsterdam, the Netherlands
[2]SRON Netherlands Institute for Space Research, Utrecht, the Netherlands
[3]Wageningen University, Meteorology and Air Quality Section, Wageningen, the Netherlands
[4]Royal Netherlands Meteorological Institute, R&D Satellite Observations, de Bilt, the Netherlands
[5]Vrije Universiteit, Department of Physics and Astronomy, Amsterdam, the Netherlands
[6]TNO, Department of Climate, Air and Sustainability, Princetonlaan, the Netherlands
[7]Institute for Marine and Atmospheric Research Utrecht, Utrecht University, Utrecht, the Netherlands

Correspondence to: Srijana Lama (s.lama@vu.nl and sreejanalama@gmail.com)

Abstract. This study investigates the use of co-located NO_2 and CO retrievals from the TROPOMI satellite to improve the quantification of burning efficiency and emission factors over the mega-cities of Tehran, Mexico City, Cairo, Riyadh, Lahore and Los Angeles. Efficient combustion is characterized by high NOx ($NO+NO_2$) and low CO emissions, making the NO_2/CO ratio a useful proxy for combustion efficiency. Local enhancement of CO and NO_2 above megacities are well captured by TROPOMI at short averaging times compared to previous satellite missions. In this study, the Upwind Background and Plume rotation methods are used to investigate the accuracy of satellite derived $\Delta NO_2/\Delta CO$ ratios. The column enhancement ratios derived using these two methods vary by 5 to 20 % across the selected megacities. TROPOMI derived column enhancement ratios are compared with emission ratios from the EDGAR v4.3.2 and MACCity, 2018 emission inventories. TROPOMI correlates strongly (r = 0.85 and 0.7) with EDGAR and MACCity showing the highest emission ratio for Riyadh and lowest for Lahore. However, inventory derived emission ratios are higher by 60 to 85 % compared to TROPOMI column enhancement ratios across the six megacities. The short lifetime of NO_2 and different vertical sensitivity of TROPOMI NO_2 and CO explain most of this difference. We present a method to translate TROPOMI retrieved column enhancement ratios into corresponding emission ratio, accounting for these influences. Except for Los Angeles and Lahore, TROPOMI derived emission ratios are close (within 10 to 25%) to MACCity. For EDGAR, however, emission ratios are higher by ~65 % for Cairo, 35 % for Riyadh. For Los Angeles, EDGAR and MACCity are higher by a factor 2 and 3 respectively compared to TROPOMI. The air quality monitoring networks in Los Angeles and Mexico City are used to validate the use of TROPOMI. For Mexico City and Los Angeles, these measurements are consistent with TROPOMI derived emission ratios, demonstrating the potential of TROPOMI to monitor burning efficiency.

1 Introduction

The rapid urbanization and economic growth in developing countries has led to a strong increase in urban air pollution (Pommier et al., 2013; United Nations, 2018). In the south Asian cities of Kabul and Dhaka, for instance, nitrogen dioxide

(NO_2) increases have been reported in the order of 10 % yr^{-1} (Schneider et al., 2015). In New Delhi, emissions of carbon monoxide (CO) increased by 22.4 % in the period 2000 to 2008 (Jiang et al., 2017). In European countries, on the other hand, the use of modern technology and other air pollution abatement measures have decreased NO_2 concentrations by 10 to 50 % in the period of 2004 to 2010 (Castellanos and Boersma, 2012) and CO by 35 % between 2002 to 2011 (Guerreiro et al., 2014). To develop effective air pollution control strategies, accurate information on local emission sources and combustion processes is important (Borsdorff et al., 2018a; Ma and van Aardenne, 2004). However, developing countries and remote areas lack the local infrastructure needed to obtain detailed information e.g. about energy consumption, fuel type and technology. Limited process information contributes largely to the uncertainty in emission inventories (Silva and Arellano, 2017). For example, the range of uncertainty in the Chinese NOx and CO emissions in the period of 2005 to 2008 has been estimated at - 20 to +45% due to inadequate information about fuel consumption and uncertain emission factor (Zhao et al., 2011, 2012). In the global emission inventory EDGAR v4.3.2, uncertainties in regional emissions have been estimated at 17 to 69% for NOx, and 25 to 64% for CO (Crippa et al., 2016). In this study, we investigate the use of satellite remote sensing to improve the emission quantification for these important air pollutants.

In global emission inventories, combustion related emissions are computed as the product of the amount of fuel burned (activity data), and the composition of the emissions as represented by the emission factor (EF) (Vallero, 2007). Emission factors depend strongly on the burning conditions (Sinha et al., 2003; Ward et al., 1996; Yokelson et al., 2003), in particular on the combustion efficiency (CE). CE is defined as the fraction of reduced carbon in the fuel that is directly converted into CO_2 (Yokelson et al., 1996). Usually, emission factors are measured in laboratories under controlled burning conditions. However, in ambient environment, combustion conditions are highly variable (Andreae and Merlet, 2001; Korontzi et al., 2003) introducing large uncertainties in global emission inventories through the impact of CE on EF. A case study (Frey and Zheng, 2002) for NOx emission estimates from the coal fired power plants with dry-bottom wall-fired boilers using low NOx burner showed that the EF for NOx can vary by factor of 4 or more within a same technology. The application of mean EFs introduces uncertainties in the range of -29 % to +35 % with respect to mean emission estimates (Frey and Zheng, 2002). Fuel type, fuel composition, combustion practices and technology are the main factor influencing combustion efficiency in the ambient environment (Silva and Arellano, 2017; Tang et al., 2019). To improve the accuracy of global inventories, a better quantification of combustion efficiency and EFs is needed.

In recent years, the availability of atmospheric composition measurements from Earth orbiting satellites has strongly improved. Sensors such as Scanning Imaging Absorption spectroMeter for Atmospheric Chartography (SCIAMACHY) (Bovensmann et al., 1999) and Tropospheric Monitoring Instrument (TROPOMI) (Veefkind et al., 2012) deliver global datasets of multiple species. The satellite observations from SCIAMACHY have been used in combination with inverse modelling techniques to test and improve emission inventories (Konovalov et al., 2014; Mijling and van der A, 2012; Reuter et al., 2014; Silva et al., 2013). By combining observations of different species (e.g. CO, CO_2, NO_2) information about common sources is obtained, and potentially also about emission ratios (Hakkarainen et al., 2015; Miyazaki et al., 2017; Reuter et al., 2019; Silva and Arellano, 2017).

In this study, measurements from the TROPOMI are used to investigate the burning efficiency in megacities. TROPOMI is a push broom grating spectrometer on board of Sentinel 5 Precursor launched by ESA on 13 October, 2017 (Veefkind et al., 2012). We use the ratio of the TROPOMI retrieved tropospheric column of NO_2 and the total column of CO, which is formally not equivalent to combustion efficiency but can nevertheless serve as a useful proxy of the burning conditions (Silva and Arellano, 2017; Tang and Arellano, 2017). The reason for this is that the NO_x emission increases with combustion temperature, which is high during efficient combustion. In contrast, CO is a product of incomplete combustion, and is produced when combustion efficiency is low (Flagan and Seinfeld, 1988). The combination of these effects makes the NO_2/CO ratio highly sensitive to combustion efficiency. To correct for differences in the NO_2 and CO background concentrations, the enhancement ratio $\Delta NO_2/\Delta CO$ is used. Here ΔNO_2 and ΔCO represent concentration increases compared with their respective backgrounds. The $\Delta NO_2/\Delta CO$ ratio is insensitive to atmospheric transport, as NO_2 and CO emissions are dispersed in a similar manner by the wind. Therefore, the impact of transport cancels out in the ratio. Because of this, TROPOMI observed ratios close to emissions sources can be directly related to emission ratios. The aim of this study is to investigate the local relation between TROPOMI retrieved $\Delta NO_2/\Delta CO$ ratios and emission ratios in a quantitative manner, focusing on megacities showing significant concentration enhancements in the TROPOMI data. In the past studies, NO_2 from the Ozone Monitoring Instrument (OMI) and CO from Measurement of Pollution in the Troposphere (MOPITT) have been used to derive CO/NO_2 ratios(Silva and Arellano, 2017; Tang and Arellano, 2017). MOPITT also has a SWIR channel (or near IR) and the multispectral (TIR/NIR) product, with near-surface sensitivity over some land regions, was used in both Silva and Arellano, 2017; Tang and Arellano, 2017. TROPOMI provides a unique opportunity to measure CO and NO_2 using the same instrument at unprecedented high spatial resolution (7x7 km^2 at nadir) and daily global coverage (Borsdorff et al., 2018b; van Geffen et al., 2019) making this instrument ideally suited for investigation of NO_2/CO ratios from space. Additionally, TROPOMI CO retrievals make use of the short-wave infrared, improving the sensitivity to surface emissions of CO compared to the thermal infrared sounders MOPITT and Infrared Atmospheric Sounding Interferometer (IASI). However, TROPOMI NO_2 retrievals are less sensitive to the lower troposphere, causing $\Delta NO_2/\Delta CO$ to be influenced by vertical sensitivity(Eskes and Boersma, 2003). We derived a correction factor to take this influence into account, as will be explained in detail in Section 2.5.

This paper is organized as follows: Section 2 provides detailed information about the TROPOMI CO and NO_2 retrieval, the approach used to quantify the $\Delta NO_2/\Delta CO$ column enhancement ratio over megacities, and how to relate it to the corresponding emission ratio. Results comparing satellite and emission inventories derived ratios are presented in section 3. Finally, section 4 summarizes our findings and presents the main conclusions.

2 Data and Method

2.1 TROPOMI CO retrievals

For this study, we are using the TROPOMI CO scientific beta data product provided by SRON (ftp://ftp.sron.nl/open-access-data-2/TROPOMI/tropomi/co/7_7/). The output is identical to the one of European Space Agency (ESA) 's operational data

product but provides in addition the TM5 a priori profiles (http://tm5.sourceforge.net/) that are used in the retrieval. The SRON CO product also supplies more data for the early months of the mission which are not included in the operational product. Total column densities of CO [molecules/cm^2] are retrieved from spectral radiance measurements from the TROPOMI short wave infrared (SWIR) module at 2.3 μm using the SICOR algorithm (Landgraf et al., 2016a). In this profile scaling algorithm, the TROPOMI observed spectra are fitted by scaling a reference vertical profile of CO using the Tikhonov regularization technique (Borsdorff et al., 2014). The reference a priori CO profile is derived from the TM5 transport model (Krol et al., 2005) as described in Landgraf (2016b). The averaging kernel (A) is an essential component of the CO retrieval, which quantifies the sensitivity of the retrieved CO column to a change in the true vertical profile (ρ_{true}) following Borsdorff et al., (2018c), as

$$C_{retrieval} = A * \rho_{true} + \epsilon_{CO} \quad (1)$$

Where, ϵ_{CO} is the error in the retrieved CO columns.

2.2 TROPOMI NO_2 retrievals

The UV-Vis module of TROPOMI is used to retrieve NO_2 in the 405-465nm spectral range. NO_2 slant column densities are processed using the TROPOMI NO_2 DOAS software developed at KNMI (van Geffen et al., 2019). The retrieval algorithm is based on the NO_2 DOMINO algorithm (Boersma et al., 2011) which has been improved further in the QA4ECV4 project (Boersma et al., 2018). The algorithm subtracts the stratospheric contribution to the slant column densities, and then converts the residual tropospheric slant column density into the tropospheric vertical density via the air mass factor (AMF). The AMF is computed using co-sampled, daily NO_2 a priori vertical profiles from output of the TM5-MP chemistry transport model at 1˚ x 1˚ resolution (Williams et al., 2017). AMF depends on the surface albedo, terrain height, cloud height and cloud fraction (Eskes et al., 2018; Lorente et al., 2017). We have used the offline level 2 NO_2 data [molem^{-2}] available at (https://s5phub.copernicus.eu; http://www.tropomi.eu). The TROPOMI NO_2 product has been successfully used in various studies so far (Griffin et al., 2019; Reuter et al., 2019). There are indications that NO_2 is biased low by approximately 30% in the tropospheric columns because of issues with the cloud pressure and the a priori NO2 profile used in the AMF calculation (Boersma et al., 2004; Lorente et al., 2017).

2.3 Data Selection

We used TROPOMI CO and NO_2 retrievals from June to August, 2018 because of the large number of clear sky days during this period over megacities of our interest. Megacities are strong sources of air pollution and can readily be observed in TROPOMI data (Borsdorff et al., 2018c). Since CO and NO_2 are retrieved from different instrument channels using different algorithms, the filtering criteria and spatial resolutions are also different. To facilitate data filtering, both algorithms provide a quality assurance value (qa value). The qa value for both products ranges from 0 (no data) to 1 (high quality data)

For our data analysis, we selected NO_2 retrievals with qa values equal or larger than 0.75, indicating clear sky conditions (Eskes and Eichmann, 2019), and CO retrievals with qa values equal or larger than 0.7, representing measurements under clear sky

conditions or the presence of low-level clouds (Apituley et al., 2018). The application of the SICOR algorithm to SCIAMACHY CO retrievals with low-level clouds increases the number of measurement, with a limited impact in the ability to detect CO sources (Borsdorff et al., 2018a).CO retrievals are filtered for stripes as described in Borsdorff et al., (2018c).
135 The CO retrieval has a factor 2 coarser spatial resolution than the NO_2 retrieval (7x7km2 versus 3.5x7km2). To collocate NO_2 and CO retrievals, we combine those NO_2 pixels which centres fall within a CO pixel, selecting only those pixels for which both the NO_2 and CO retrievals pass the filtering criteria. The total CO column and tropospheric NO_2 columns are converted into the dry column mixing ratio XCO (ppb) and XNO_2 (ppb) using the dry air column density calculated using the collocated surface pressure data included in the CO data files as described in Borsdorff et al., (2018c).

140

Table 1. Selected megacities and specifications used for emission ratio quantification

City	Centre (Latitude, Longitude)	Radius of core city (km)	Radius outskirt (km)	Radius background (km)	Upwind area Δlat, Δlon (˚)
Tehran	35.68, 51.42	10	180	250	1.0, 1.0
Mexico City	19.32, -99. 20	10	170	180	1.0, 1.0
Cairo	30. 04 31.23	10	135	180	1.0, 1.0
Riyadh	24.63, 46.71	10	100	150	1.0, 1.0
Lahore	31.53, 74.35	10	100	150	1.0, 1.0
Los Angeles	34.05, -118.24	10	200	250	1.0, 1.0

2.4 Calculation of NO_2/CO

This study focuses on the following megacities (population > 5 million): Mexico City, Tehran, Riyadh, Cairo, Lahore and Los Angeles. These six megacities are well isolated from surrounding sources and frequently experience cloud-free conditions,
145 allowing the retrieval of a large number of XCO and XNO_2 data from TROPOMI. Los Angeles and Mexico City have automated air quality monitoring networks, measuring CO and NO_2 at different locations in the city. These measurements are used in section 3.3 to validate the results obtained using TROPOMI. In addition, these megacities are expected to span a

sizeable range in burning efficiency by including urban centres in developed (US/ Los Angeles) and developing countries (Mexico/ Mexico City, Egypt/ Cairo, Saudi Arabia/Riyadh, Pakistan/ Lahore).

The concentration gradient between the background and the city centre is used to determine the $\Delta XNO_2/\Delta XCO$ enhancement ratio. To determine this ratio, we divide each city into a core city area and a background area. Every city has a different size and different neighbouring CO and NO2 emission sources and therefore the appropriate choice of radii for the background and outskirt areas varies between cities (see Supplements Section 1 for details). Since the same regional definition is used for NO2 and CO, the enhancement ratio is not sensitive to the details of the region selection. Most important for the choice of radii is to catch the local enhancement in CO and NO2 to its full extend, to optimize the signal over noise and thereby detection limit for urban emissions. To maximize the size of the city enhancement, we exclude the diffuse outskirt area in between the city centre and the background. For the location of the city centre we use the weighted average emission centre of NO_2, derived from the EDGAR emission database (Dekker et al., 2017). The derived centre coordinates, and the radii of the city core and background area are listed in Table 1. We test the robustness of the satellite-derived emission ratio using two different methods, which are explained in detail below.

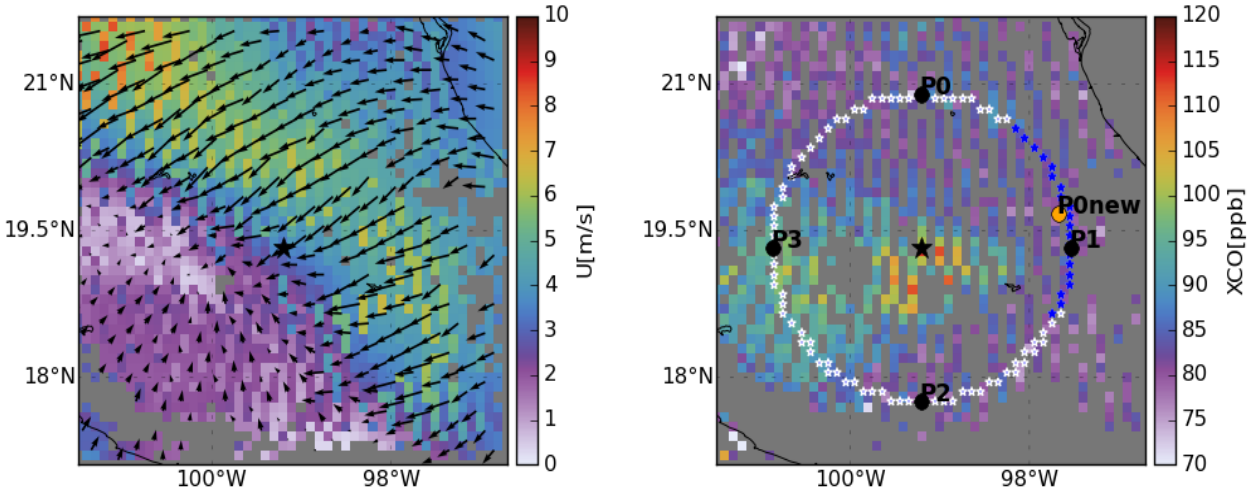

Figure 1. Average wind speed and direction from the surface to 200m from ERA Interim at the time of TROPOMI overpasses (left) and TROPOMI derived total column CO over Mexico City (right) for June 4th, 2018. The black star represents the centre of the city. In the right panel, the white circle is the background area for Mexico City and the blue section represents the upwind background area that we selected depending upon the wind direction (θ) in the core city area. P0, P1, P2 and P3 are the points where the north, east, west and south wind directions intersect with the background area. $P0_{new}$ is the new point generated by rotating P0 with θ in reference to the city centre

2.4.1 Upwind background

To determine the upwind background (UB) column mixing ratio, we select a section of the background region that is upwind from the city centre using the average wind direction over the core city area (see Fig. 1 and Fig. S7 for further details).

Generally, more than 75% of all pollutants are emitted between the surface and 200m altitude (Bieser et al., 2011). Therefore, average wind speed and direction from surface to 200m altitude are derived from the ERA-interim reanalysis, provided at 0.75˚x0.75˚ and 3 hourly resolutions. The wind vector components of ERA-interim are spatially and temporally interpolated to the central coordinate of TROPOMI pixels. Using this information, daily enhancement ratios are calculated as follows.

$$\Delta XNO_2 = XNO_{2_{city}} - XNO_{2_{background}} \quad (2)$$

$$\Delta XCO = XCO_{city} - XCO_{background} \quad (3)$$

$$Ratio = \frac{\Delta XNO_2}{\Delta XCO} \quad (4)$$

The background area might contain free tropospheric NO_2 from lightning and convectively lofted surface NO_2 from elsewhere. However, these contributions vary on scales that are usually large compared with the scale of a city. Therefore, the calculated ΔXNO_2 and ΔXCO enhancements are caused predominantly by emissions from the city.

2.4.2 Plume Rotation

The daily TROPOMI-observed city images are rotated in the direction of wind using the city centre as the rotation point to align each CO and NO_2 plume in upwind-downwind direction (Pommier et al., 2013). Rotated images for June to August 2018 are averaged together (see Fig. S8). ΔXNO_2 and ΔXCO are determined by subtracting the average of the first quartile XNO_2, XCO values in a 100 km x 20 km region upwind from the city centre from the average of the fourth quartile XNO_2, XCO values in a 100 km x 20 km region downwind from the city centre. Finally, the enhancement of XNO_2 and XCO is calculated as described in Eq. (5) and the enhancement ratio is derived by using Eq. (4).

$$downwind - upwind\ difference = Vd - Vu = \frac{\sum_{i=1}^{n\ downwind}(X \geq 75^{th}\ percentile)}{n_{\ downwind}} - \frac{\sum_{i=1}^{n\ upwind}(X \leq 25^{th}\ percentile)}{n_{upwind}} \quad (5)$$

where, $n_{downwind}$ = number of observations ≥ 75th percentile, n_{upwind} = number of observations ≤ 25th percentile

2.5 NO_2/CO emission ratio

Local TROPOMI derived ratios in column abundance are compared with emission ratios derived from the Emission Database for Global Atmospheric Research (EDGAR v4.3.2) at 0.1˚ x 0.1˚ spatial resolution for the most recent year of 2012 and the database provided by Monitoring Atmospheric Chemistry and Climate and CityZen (MACCITY), for 2018 available at 0.5˚ x 0.5˚ resolution (Granier et al., 2011). MACCity has been re-gridded to a spatial resolution of 0.1˚ x 0.1˚ assuming a uniform distribution of the emissions within each 0.5˚ x 0.5˚ grid box. Both emission inventories contain total emissions of NOx and CO. NOx emissions are converted into NO_2 by dividing NOx by the conversion factor of 1.32. This conversion factor is based on Seinfeld and Pandis (2006) and represents urban plumes at 13.30 local time. The emission ratio of NO_2 and CO (E_{NO2}/E_{CO})

is calculated from total emissions (sum of all processes) within the core city area, for the EDGAR and MACCity emission inventories.

To compare TROPOMI to inventory derived ratios, the NO_2 tropospheric column has to be corrected for its limited atmospheric residence time. The CO lifetime is long enough compared with the transport time out of the city domain to be neglected. In addition, we need to account for differences in the vertical sensitivity of TROPOMI to NO_2 and CO, as quantified by their respective averaging kernels (A) shown in Fig. 2. To compare TROPOMI to EDGAR and MACCity, we formulate a relationship between the emission ratio (E_{NO2}/E_{CO}) and the column enhancement ratio ($\Delta XNO_2/\Delta XCO$) taking into account the combined effect of atmospheric transport, chemical loss and the averaging kernel. This relationship is as follows (see Appendix A for its derivation).

$$\frac{E_{NO2}}{E_{CO}} = \frac{\Delta XNO_2}{\Delta XCO} \frac{\left(\frac{U}{lx} + K[OH]\right)}{\frac{U}{lx}} \cdot \frac{1}{(1 - A_{influence})} \quad (6)$$

Where, U is the is the 200m wind speed (ms^{-1}), lx is diameter of the city centre (m), K is the rate constant of the reaction of NO_2 with OH *of* $2.8e^{-11}\left(\frac{T}{300}\right)^{-1.3}$ cm^3 $molecule^{-1}$ s^{-1} (Burkholder et al., 2015). T (K) and OH (molecule cm^{-3}) are respectively the boundary layer average temperature and OH concentration and $A_{influence}$ is the influence of the averaging kernel on $\Delta XNO_2/\Delta XCO$ (see section 3.2).

OH, CO and NO_2 fields from the Copernicus Atmospheric Monitoring Service (CAMS) real time are used to account for the impacts of chemical loss and the averaging kernel. The CAMS data, at 0.1° x 0.1° and 3 hourly resolution, are spatially and temporally interpolated to the TROPOMI footprints. CAMS CO and NO_2 vertical mixing ratio profiles are converted into vertical column densities using ERA Interim reanalysis surface pressure. For CO, the TROPOMI data provide column A's from the surface to the top of atmosphere. For NO_2, tropospheric A is derived using the air mass factor for the troposphere as fraction of the total column (Boersma et al., 2016). For further details see Appendix B.

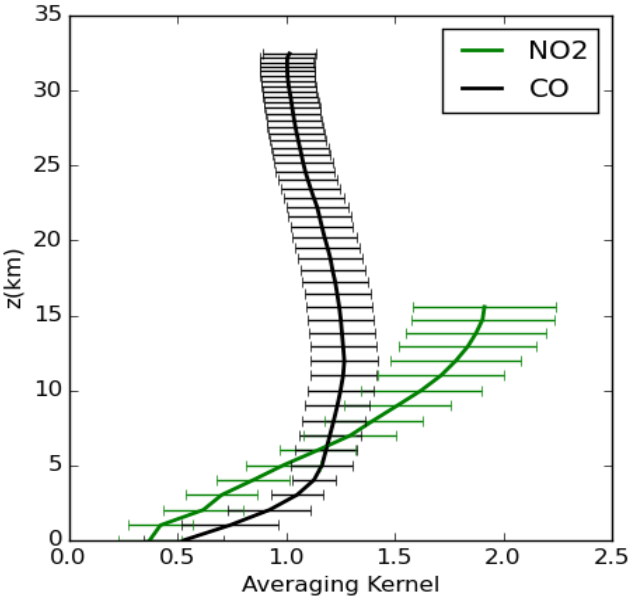

Figure 2. TROPOMI total column averaging kernels (A) for CO and tropospheric NO_2 for June 1st, 2018 over Mexico. The error bars represent the standard deviation of the mean A at each vertical level

2.6 Uncertainty

To quantify the uncertainty in TROPOMI-derived $\Delta XNO_2/\Delta XCO$ ratios for the plume rotation method, we use the error propagation method of Pommier et al.,(2013) and boot strap for the upwind background, as explained further below.

2.6.1 Bootstrapping

The boot-strapping method is a statistical resampling method, used here to calculate the uncertainty in the daily enhancement ratio of $\frac{\Delta XNO2}{\Delta XCO}$. The first step is to generate a new set of samples by drawing a random subset with replacement from the full dataset of N daily $\frac{\Delta XNO2}{\Delta XCO}$ ratios. The subset has the same number of samples as the full dataset, from which a mean ratio is calculated. This procedure is repeated a thousand times for each city. Finally, the standard deviation of the resulting ratios is taken and used to represent the uncertainty in daily $\frac{\Delta XNO2}{\Delta XCO}$.

Error propagation

To calculate the uncertainty in $\frac{\Delta XNO2}{\Delta XCO}$ by error propagation, we first determine the uncertainty in the enhancements ΔXNO_2 and ΔXCO, which are derived from the uncertainty in the mixing ratios upwind and downwind of the source as follows

$$\sigma_{\Delta X} = \sqrt{\left(\frac{\sigma_{upwind}}{\sqrt{n_{upwind}}}\right)^2 + \left(\frac{\sigma_{downwind}}{\sqrt{n_{downwind}}}\right)^2} \qquad (7)$$

where, X is XNO_2 or XCO.

Here, we assume that the upwind and downwind uncertainties are independent. The uncertainty for the column enhancement is:

$$\sigma_{ratio} = \left(\sqrt{\left(\frac{\sigma_{\Delta NO_2}}{\Delta XNO_2}\right)^2 + \left(\frac{\sigma_{\Delta CO}}{\Delta XCO}\right)^2}\right) * \frac{\Delta XNO_2}{\Delta XCO} \qquad (8)$$

3 Results and Discussion

3.1 Detection of NO_2 and CO pollution over megacities

The collocated TROPOMI XNO2 and XCO data have been averaged for June to August 2018, for domains of 500 x 500 km2 centred around the selected megacities as described in section 2. Results are shown in Fig. 3 for Mexico City and Cairo. The enhancements of XCO and XNO2 over Mexico City and Cairo are clearly separated from the surrounding background areas and are prominent in several overpasses of TROPOMI (Fig. S9). This demonstrates that a relatively short data averaging period is sufficient for TROPOMI to detect hotspots of CO pollution at the scale of large cities, compared to instruments such as IASI and MOPITT. The orography surrounding Mexico City causes trapping of pollutants facilitating detection by TROPOMI. The longer lifetime of CO compared to NO2 causes the urban influence of CO to be propagated further in westward direction. As can be seen in Fig. 3, the retrieved XCO and XNO2 signals of emissions from Mexico City and Cairo correlate quite well with each other, confirming that it should be possible to obtain useful information about burning efficiency by studying $\frac{\Delta XNO2}{\Delta XCO}$. An industrial area is located to the east of Cairo (29.797351N, 32.148266 E), showing a clear enhancement in XNO2 but not in

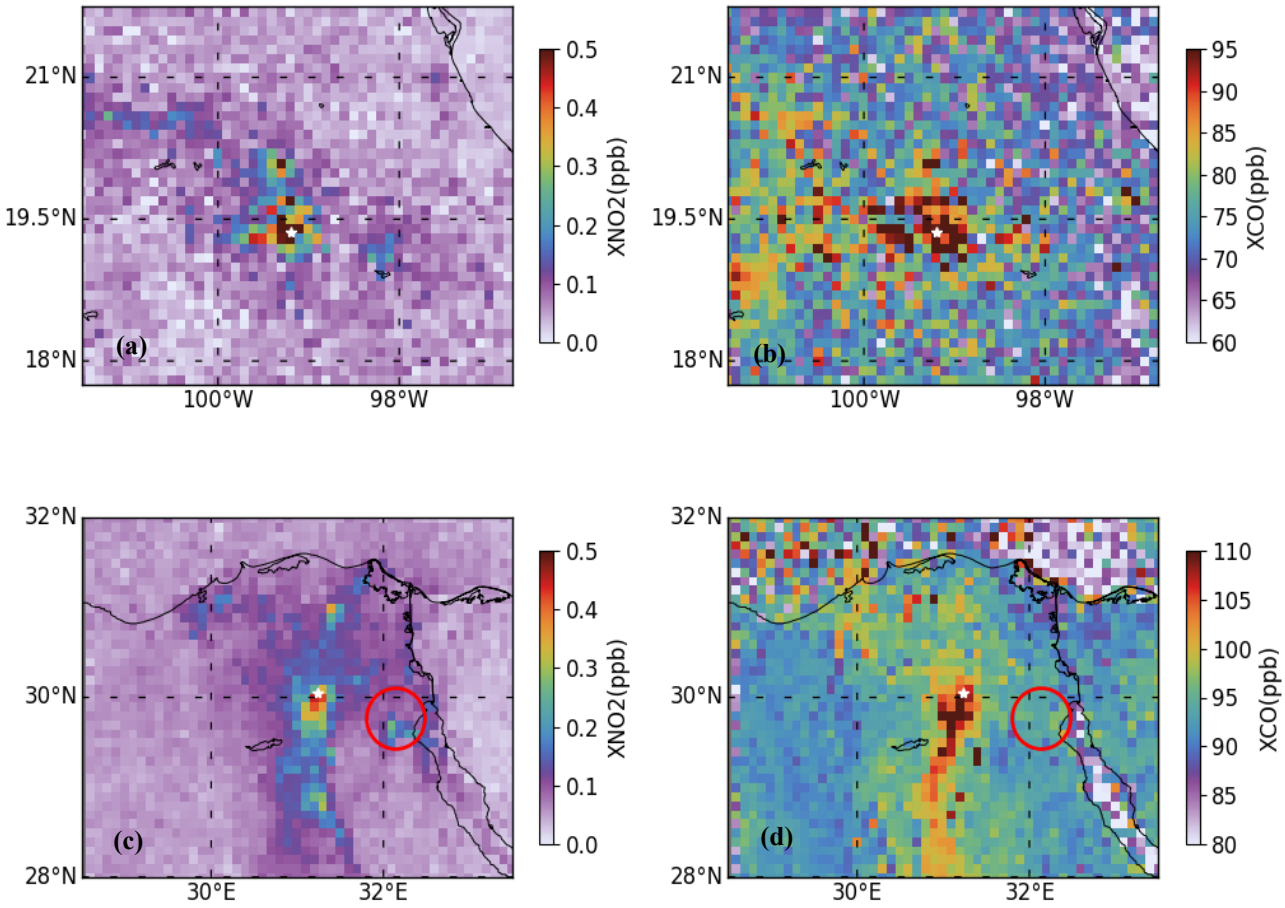

Figure 3. Collocated TROPOMI retrieved XNO_2 (left) and XCO (right) data over Mexico (top) and Cairo (bottom) averaged for June to August, 2018. De-striping is applied to CO total columns (Borsdorff et al., 2018b) and CO and NO_2 retrievals have been re-gridded to 0.1˚x0.1˚. The white stars represent the centres of Mexico City and Cairo, respectively. The red circle in panels c) and d) points to an industrial area eastward of Cairo.

XCO (Fig. 3c and d). It demonstrates that variations in the column enhancement ratio can already be seen by eye comparing TROPOMI retrieved XCO and XNO2 images.

3.2 Comparison between TROPOMI and inventory derived ratios

In this subsection, we attempt to compare TROPOMI-derived NO_2/CO column enhancement ratios to emission ratios from EDGAR and MACCity for the six selected megacities (see Fig. 4). As explained in section 2, column enhancement ratios from TROPOMI are obtained using the upwind background (UB) and plume rotation (PR) methods. These estimates differ by 5 to 20 % across the six cities, providing an initial estimate of the accuracy at which the column enhancement ratio can be derived (see Table S1 for details). The EDGAR and MACCity inventories show a substantial variation in emission ratios between cities, with relatively high emission ratios for Riyadh and the lowest for Lahore. TROPOMI-derived $\Delta XNO_2/\Delta XCO$

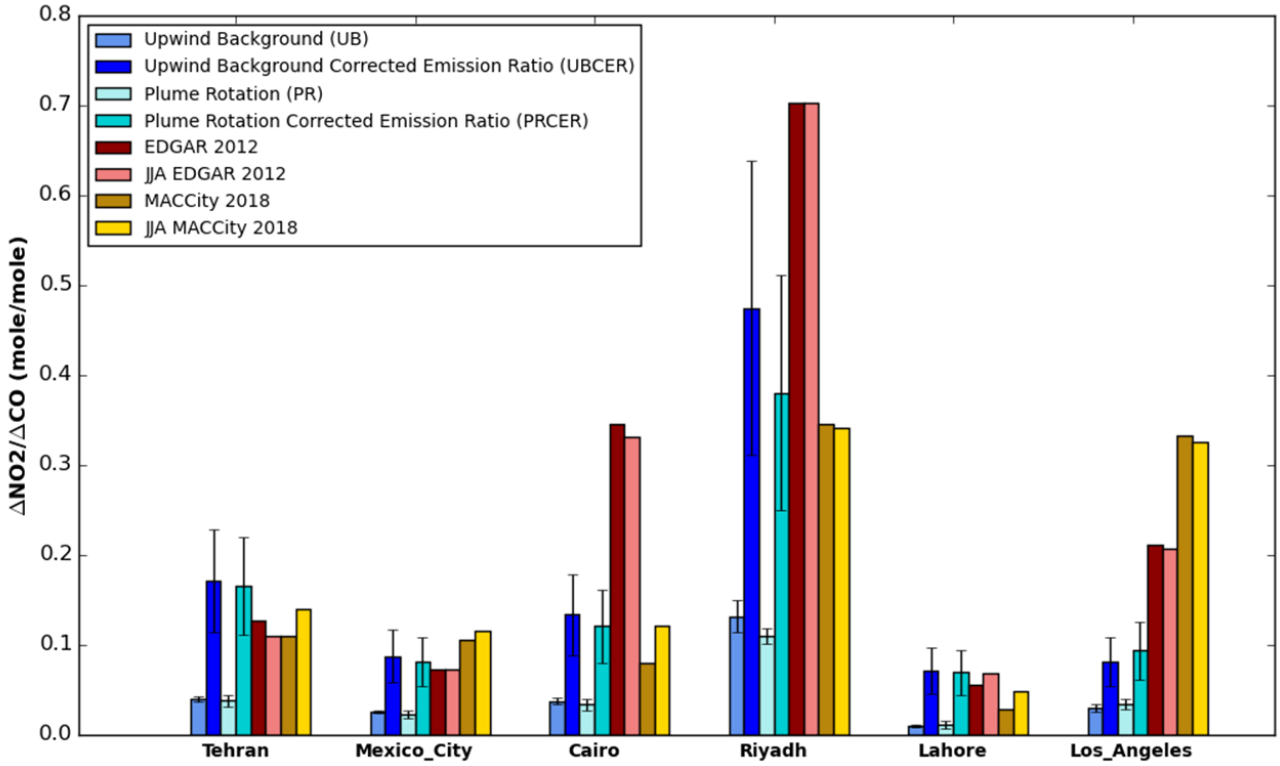

Figure 4. Comparison of TROPOMI-derived $\Delta NO_2/\Delta CO$ enhancement ratios, calculated using different methods shown in blue shades, to corresponding emission ratios from the EDGAR (red shades) and MACCity (yellow shades) emission inventories for six megacities. Dark solid shades for emission inventories represent the annual average inventory derived ratio, whereas faded shades represent June to August averaged inventory derived ratios. The upwind background corrected emission ratio (UBCER) and Plume rotation corrected emission ratio (PRCER) account for the impact of photochemical NO_2 removal and the averaging kernel. Error bars for TROPOMI-derived $\Delta NO_2/\Delta CO$ enhancement ratios represent 1σ uncertainties calculated using boot strapping (upwind background) and error propagation (plume rotation method). The error bar for UBCER and PCER accounts the uncertainty in methodology and TROPOMI data (for details see Table S3).

column enhancement ratios for the UB and PR methods show similar patterns as EDGAR and MACCity with Pearson correlation coefficients of 0.85 and 0.7 respectively (Fig. S10). However, inventory-derived emission ratios are clearly larger than TROPOMI-derived column enhancements ratios by 60 to 85%, explained largely by the impact of the limited NO2 lifetime and the averaging kernel, as will be discussed further after explaining the differences between EDGAR and MACCity. Emission ratios from MACCity are lower than from EDGAR by 10 to 75%. To understand the differences in emission ratios between MACCity and EDGAR, we selected two cities, Cairo and Mexico City, which present the largest and smallest differences in emission ratio. The CO and NO_2 emissions are categorized into seven sectors: agriculture, residence, energy, industries, transportation, shipping and waste treatment. Sectors are compared that contribute most to the total emission. In the case of Cairo and Mexico City these are the transportation, industries, energy and resident sectors (Fig. S11a and b). For Cairo, the total CO emission is lower in EDGAR than in MACCity by a factor 2, whereas the total NO_2 emission is 10% higher in

EDGAR. This results in an emission ratio that is higher by a factor 3. The largest discrepancy between EDGAR and MACCity CO emission is due to the resident sector followed by energy. For NO_2, the energy, transportation and resident sectors explain most of the difference between EDGAR and MACCity. In Mexico City, EDGAR total CO and NO_2 emission are both higher by a factor 2 compared to MACCity, cancelling out in the ratio leading to the best agreement of all selected megacities. However, it is complicated to identify the main factors explaining the differences between EDGAR and MACCity at the sector level due to the combined influence of differences in activity data, emission factors and the methods used to disaggregate country totals. To understand the disaggregation of emission in EDGAR and MACCity, we compared the country total CO and NO_2 of Mexico/ Mexico City and Egypt/ Cairo. The comparison shows that EDGAR and MACCity country CO total and NO_2 total of Mexico shows a small differences (~12%) whereas in Mexico city the difference is about factor of 2 (Fig. S11c). For Egypt, EDGAR and MACCity CO total shows the similar differences as Cairo whereas EDGAR NO_2 country total emission is lower by factor 2 (Fig. S11d). This shows that EDGAR attribute CO and NO2 emission to the city and MACCity smears them out over the country.

The difference between satellite-derived column enhancement ratios and inventory-based emission ratios can be explained in part by the relative short lifetime of NO_2, reducing columnar NO_2/CO ratios compared to the emissions. In addition, the sensitivity to the planetary boundary layer is smaller for NO_2 than for CO TROPOMI measurements, reducing the satellite observed column enhancement ratio further. Taking these influences into account using Eq. (6) leads to the Upwind Background Corrected emission ratio (UPCER) and Plume rotation Corrected Emission Ratio (PRCER) in Fig. 4, which have been calculated on a daily basis before averaging over the full period. Due to the short lifetime of OH, its concentration depends strongly on the local photochemical conditions (de Gouw et al., 2019). Therefore, to account for the local lifetime of NO_2, we need an estimate of the OH that is representative for the photochemical conditions inside cities. Figure 5 shows the boundary layer OH concentration at the time TROPOMI overpasses from CAMS for Mexico City, averaged over June-August, 2018. The Fig.5 shows a clear enhancement of OH in the city centre, confirming that the spatial resolution of CAMS is sufficient to resolve urban influences on OH in megacities. UB and PR column enhancement ratios increase by 60 to 85 %, when accounting for the NO_2 lifetime (see Table S1). The boundary layer OH concentrations and mean wind speeds for the six cities are listed in Table 2.

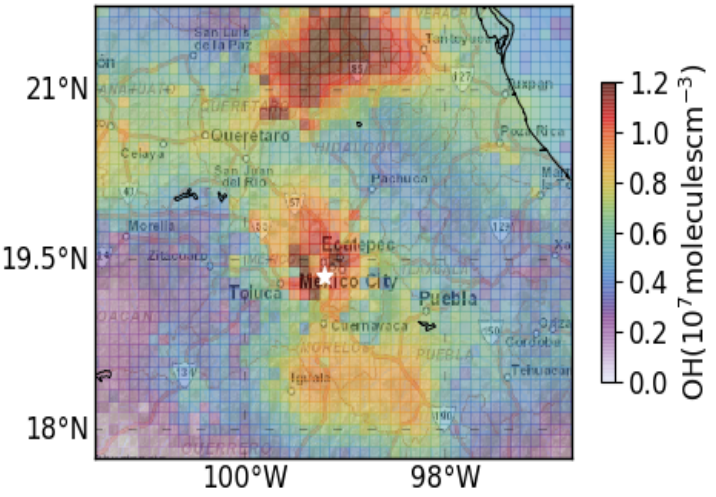

Figure 5. The boundary layer average OH concentration at the time of TROPOMI overpasses during June to August, 2018 over Mexico City. The white star represents the centre of Mexico City.

The impact of differences between the XNO_2 and XCO averaging kernels, is calculated using vertical profiles of NO_2 and CO taken from CAMS. These profiles were used to calculate XNO_2 and XCO using either the TROPOMI A's or A's replaced by identity matrices. The relative difference $A_{influence} = \frac{(Without\ A - with\ A)}{Without\ A}.100\%$ quantifies the impact of differences between the averaging kernels (see Appendix C for the derivation). The CAMS simulated city enhancements for CO over June to August, 2018 did not compare well with TROPOMI for Tehran, Cairo, Riyadh and Lahore, possibly due to the coarse resolution of CAMS (see Fig. S14, S15, S16 and S17). Therefore, $A_{influence}$ has been determined for Mexico City and Los Angeles to calculate the averaging kernel impact (Fig. S12 and S13). To test the accuracy of $A_{influence}$, a few days for Tehran, Cairo, Riyadh and Lahore were selected when CAMs CO and NO_2 enhancements did compare relatively well with TROPOMI. For the six megacities, TROPOMI derived $\Delta NO_2/\Delta CO$ ratios are 10 to 15 % lower than the 'ideal' $\Delta NO_2/\Delta CO$ ratio that would be measured if both retrievals had uniform vertical sensitivities, i.e. every molecule in the column receives equal weight. Details about the selected days, and calculated corrections for each city are listed in Table S2.

After correction, UBCER and PRCER for Tehran and Mexico City are close to EDGAR and MACCity (10 to 25%). This confirms that the emission factors for these cities are well represented in the EDGAR and MACCity emission inventories. The difference between corrected and uncorrected ratios in Fig. 4 highlights the importance of the correction, in particular the influence of OH, for assessing emission ratios using TROPOMI. For Cairo the correction also reduces the difference between TROPOMI and the emission inventories, although the EDGAR ratios remain higher by about 65 % for Cairo than UBCER and PRCER. For MACCity, the emission ratios are close to TROPOMI derived UBCER and PRCER for Cairo (within 20 %), pointing to a more accurate representation of emission ratios in MACCity than in EDGAR. For Riyadh UBCER and PRCER are close to MACCity (~10 to 20 %) whereas EDGAR is higher by 35%. However, for Lahore, PRCER is close to the EDGAR ratio, whereas MACCity is lower by a factor of 2.5. For Los Angeles, the ratios from EDGAR and MACCity are higher by 55 % and 70 % respectively than UBCER and PRCER after correction, suggesting poorer burning conditions than represented by the emission inventories. To further investigate this discrepancy for Los Angeles, we included the Hemispheric Transport of Air pollution version 2 (HTAP-v2) emission inventories for 2010 in the comparison. HTAP-v2 has a resolution of 0.1˚ x 0.1˚ and makes use of emission estimates from the Environmental Protection Agency (EPA) for the USA (Janssens-Maenhout et al., 2015). The HTAP-v2 derived emission ratio over Los Angeles is 0.074, which is close to UBCER and PRCER (within 20 %). This result provides further confidence in TROPOMI derived emission ratio. However, different sources of uncertainty play a role as discussed further below.

Seasonal variations in emission factors may influence our comparison between seasonal averaged TROPOMI data and annual average EDGAR emissions. To account for the influence of seasonally varying emission factors, we compute a seasonal correction factor based on EDGAR v4.3.2 2010 since monthly data are not available for EDGAR 2012(see Fig.4). Except for Lahore, the June to August (JJA) EDGAR ratio is lower by 5 to 12.5 % compared to the annual average EDGAR ratio. The MACCity ratio for JJA, however, is higher by 10 to 71% compared to the annual average, indicating that EDGAR and MACCity disagree on the seasonality of the NO2/CO emission ratio. For MACCity, the agreement with TROPOMI improves

335

Table 2. Average wind speed and boundary layer CAMs OH concentration for June- August, 2018, used to correct for the limited lifetime of NO_2. The error bar represents 1σ uncertainty calculated by boot strapping method.

Cities	Mean wind speed (kmh^{-1})	Mean OH concentration (10^{7} $moleculescm^{-3}$)	Conversion factor
Tehran	12.9±*0.45*	1.77±*0.15*	1.23±*0.005*
Mexico City	11.4±*0.7*	1.0±*0.1*	1.27±*0.009*
Cairo	16.5±*0.42*	1.85±*0.14*	1.24±*0.0029*
Riyadh	21.1±*1.0*	1.6±*0.2*	1.35±*0.007*
Lahore	7.1±*0.6*	1.3±*0.2*	1.19±*0.006*
Los Angeles	15.3±*0.43*	1.2±*0.1*	1.25±*0.006*

improves the most when taking seasonality into account (see Fig.4).

340 The ozone concentration and the photolysis rate impact the partitioning of NO and NO_2 (Jacob, 1999) influencing the applied conversion factor of 1.32. To further investigate the uncertainty introduced by this factor, we analysed CAMS surface NO and NO_2 at the time of the TROPOMI overpasses (see Table 2). The CAMS-derived conversion factor varies <10 % compared with the standard value of 1.32, introducing a <10 % uncertainty in the inventory derived emission ratio. However, given the uncertainty in the CAMS simulated urban NO, NO_2 and OH concentrations (Huijnen et al., 2019) the actual uncertainty is 345 probably higher. Additionally, TROPOMI underestimates the NO_2 column by 7 % to 29.7 % relative to MAX-DOAS ground based measurement in European cities (Lambert, et al., 2019). However, since we don't know yet how representative this estimate is for the cities that we study, the impact of this bias has been accounted for as an additional source of uncertainty of 30 % in the TROPOMI inferred NO2/CO ratio (see Table S3). Compared to this number other sources of uncertainty such as the wind direction and speed (FigS18 and S19), boundary layer OH concentration (Table 2), $A_{influence}$ correction Table S2) and 350 the predefined background setting (Fig S20) make only small contributions to the TROPOMI derived emission ratio. The total uncertainty in the TROPOMI derived emission ratio is calculated using error propagation (see Table S3) and ranges between 33 to 35.6%.

We also acknowledge that our treatment of the photochemical removal of NO_2 is simplified. In reality, NO_2 is influenced by several other factors including meteorological parameters such as temperature, wind speed and radiation (Lang et al., 2015; 355 Romer et al., 2018), causing the formation and loss of NO_2 to vary spatially and temporally. In the corrected ratio, we only consider the first order loss of NO_2 by OH forming HNO_3. Several studies show that in cities surrounded by forested areas, loss of NO_2 through the formation of alkyl and multifunctional nitrates ($RONO_2$) can play a more important role than nitric acid production (Browne et al., 2013; Farmer et al., 2011; Romer Present et al., 2019; Sobanski et al., 2017). In addition, secondary production of CO from VOC oxidation may play a role. However, this only affects our ratios if it changes the CO

gradient between the city and the background. Hence, to further improve the accuracy of TROPOMI supported evaluation of emission ratios a more sophisticated treatment of urban photochemistry is required.

3.3 Validation using ground based measurements

To further evaluate TROPOMI's ability to quantify burning efficiencies, TROPOMI derived $\Delta XNO_2/\Delta XCO$ ratios have been compared with ground-based measurements from Mexico City and Los Angeles. For this purpose, twenty ground-based stations in Mexico City with hourly measurements of CO and NO_2 have been selected from the AIRE CDMX network (http://www.aire.cdmx.gob.mx/). Similarly, for Los Angeles twelve ground based stations from South Coast Air Quality Management District (AQMD) monitoring network (www.aqmd.gov/) have been selected. For the details of the names and locations of these sites see Table S4. For Mexico City, data were only available for June 2018. For Los Angeles, data for the June to August 2018 period were used but the periods 25 July to 11 August and 17 to 26 August were excluded to avoid the influence of wild fires on the observed urban pollution level. The validation results are presented in Fig. 6 for spatially averaged, hourly CO and NO_2 measurements for Mexico City and Los Angeles collected during noon (12:00 to 14:00 local time). To determine the enhancement in CO and NO_2 due to local emissions for each ground-based station, the 5th percentile of hourly CO and NO_2 measurements is used as background. ΔCO and ΔNO_2 enhancements for individual monitoring stations are calculated as $\Delta X = X_{individual} - X_{background}$.To compare with TROPOMI, all measurement sites are spatially averaged.

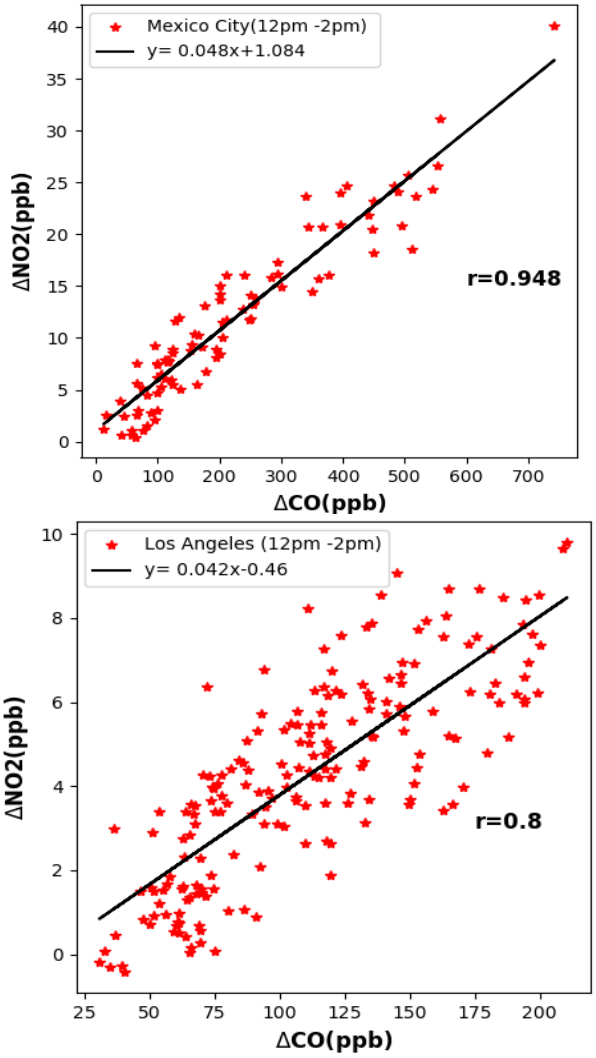

Figure 6. The relation between ΔNO_2 and ΔCO in surface measurements from Mexico (top) and Los Angeles (bottom). The red dots represent spatially averaged hourly measurements collected during the day (12:00 to 14:00 local time)

Ground based ΔCO and ΔNO_2 at Mexico City and Los Angeles are strongly correlated with a Pearson correlation coefficient of r = 0.95 and 0.80 respectively, confirming that the observed signals reflect NO_2 and CO emissions from common sources. The slope of the regression line for Mexico City amounts to 0.048, which is 45% higher than the TROPOMI derived column enhancement ratio using the UB and PR method.

The $\Delta NO_2/\Delta CO$ ratio that is observed at ground level is likely influenced less by photochemical removal of NO_2 than the TROPOMI retrieved columns, and therefore closer to the inventory derived ratio, consistent with our results. This comparison suggests that removal of NO_2 reduces the ratio in ground-based measurements by 35 % compared to EDGAR and MACCity. Overall, the emission ratios in EDGAR and MACCity for Mexico City are consistent with both the ground-based measurements and TROPOMI, i.e. within the uncertainty of introduced by the chemical removal of NO_2.

For Los Angeles, the regression slope is 0.042, which is 10 to 20% larger than the TROPOMI derived column enhancement ratios using the UB and PR method. However, the EDGAR and MACCity ratios are higher by a factor 5 compared to the $\Delta NO_2/\Delta CO$ ratio observed at ground level. The ground-based measurements point to similar ratios for Mexico City and Los Angeles, confirming the HTAP-v2 supported TROPOMI finding that the emission ratio in EDGAR and MACCity is too high for Los Angeles. Therefore, the ground-based measurements for Los Angeles provide independent support for the TROPOMI derived ratios pointing to poorer burning conditions in Los Angeles than indicated by the emission inventories, and confirm the value of TROPOMI for monitoring the burning efficiency of megacities.

For Los Angeles, the regression slope is 0.042, which is 10 to 20% larger than the TROPOMI derived column enhancement ratios using the UB and PR method. However, the EDGAR and MACCity ratios are higher by a factor 5 compared to the $\Delta NO_2/\Delta CO$ ratio observed at ground level. The ground-based measurements point to similar ratios for Mexico City and Los Angeles, confirming the HTAP-v2 supported TROPOMI finding that the emission ratio in EDGAR and MACCity is too high for Los Angeles. Therefore, the ground-based measurements for Los Angeles provide independent support for the TROPOMI derived ratios pointing to poorer burning conditions in Los Angeles than indicated by the emission inventories, and confirm the value of TROPOMI for monitoring the burning efficiency of megacities.

4. Conclusions

In this study, we investigate the use of TROPOMI XCO and XNO_2 retrievals for monitoring the burning efficiency of fossil fuel use in megacities. To improve the accuracy of the global emission inventories, the burning efficiency and emission factor is quantified using collocated XCO and XNO_2 enhancements over the megacities Tehran, Mexico City, Cairo, Riyadh, Lahore, and Los Angeles. TROPOMI is well capable of detecting XCO and XNO_2 enhancements over these megacities with relatively short averaging time and shows the expected spatial correlation.

TROPOMI derived column enhancement ratios have been compared with emission ratios from EDGAR and MACCity. The TROPOMI derived column enhancement ratios are strongly correlated with EDGAR and MACCity inventory derived emission ratios ($r = 0.85$ and 0.7) showing the highest emission ratio for Riyadh and the lowest for Lahore. This shows that Lahore has the poorest burning efficiency whereas over Riyadh, fossil fuel burning is the most efficient of all megacities that were analysed. The impact of the short NO_2 lifetime and differences in the vertical sensitivity of the TROPOMI XCO and XNO_2 retrieval on the $\Delta NO_2/\Delta CO$ enhancement ratio has been quantified. Correcting for these factors significantly improves the agreement between ratios derived from TROPOMI and emission inventories. The comparison indicates that the emission ratio

in MACCity and EDGAR is well represented for Mexico City and Tehran. For Lahore, the EDGAR emission ratio agrees better with TROPOMI, whereas for Cairo and Riyadh the MACCity emission ratios are closest to the TROPOMI derived emission ratios. Emission ratios in EDGAR and MACCity are significantly higher by 55 to 70 % compared to TROPOMI for Los Angeles. The total uncertainty on TROPOMI derived emission ratios ranges from 33 to 35.6%. The bias in S5P TROPOMI NO2 retrievals has the most important contribution to the uncertainty in the TROPOMI derived emission ratio.

TROPOMI derived $\Delta XNO_2/\Delta XCO$ column enhancement ratios for Mexico City and Los Angeles have been validated using ground-based measurement from local air quality monitoring networks. For Mexico City, the enhancement ratio derived from ground-based measurements is consistent with EDGAR, MACCity and the TROPOMI derived emission ratio. For Los Angeles, TROPOMI derived enhancement ratios are consistent with the ground-based measurements as well as the HTAP-v2 inventory based on EPA statistics, whereas EDGAR and MACCity-derived emission ratios appear to be overestimated by a factor 5 compared to ground-based measurements. This demonstrates the potential of TROPOMI data for monitoring burning efficiency and evaluating emission inventories.

Data availability: TROPOMI NO_2 and CO data are used for this paper. These data can be downloaded from https://s5phub.copernicus.eu; http://www.tropomi.eu and ftp://ftp.sron.nl/open-access-data-2/TROPOMI/tropomi/co/7_7/ . Ground based network data for Mexico and Los Angeles can be downloaded from http://www.aire.cdmx.gob.mx/ and www.aqmd.gov/ respectively. EDGAR v4.3.2, MACCity and HTAP-v2 data are available at https://eccad3.sedoo.fr/. CAMS data can be downloaded from https://apps.ecmwf.int/datasets/data/cams-nrealtime/levtype=ml/.

Author Contributions: S.L performed data analysis, interpretation and writing paper. SH supervised the study. SH, FKB, HE, IA, MK, HACDG, AJD discussed the result. TB and AL provided modified Copernicus Sentinel data 2018 CO data. All the authors commented on the manuscript and improve it.

Competing interests: The authors declare that they have no conflict of interest.

Acknowledgements: We would like to thank the team that has realized the TROPOMI instrument, consisting of the partnership between Airbus Defence and Space Netherlands, KNMI, SRON, and TNO, commissioned by NSO and ESA. Sentinel-5 Precursor is part of the EU Copernicus program, and Copernicus Sentinel data 2018 has been used. This research is funded by the NWO GO program (grant 2017.036). We thank to T.B and A.L for providing the modified Copernicus Sentinel data 2018 CO data. T.B. and A.L. are funded by the TROPOMI national programme through NSO. We thank SurfSara for making the HPC platform Cartesius available for computations through computing grant 17235. We would like to thank South Coast Air Quality Management District (AQMD) monitoring network and Calidad del aire for the free use of air quality data.

References

Andreae, M. O. and Merlet, P.: Emission of trace gases and aerosols from biomass burning, Global Biogeochem. Cycles, 15(4), 955–966, https://doi.org/10.1029/2000GB001382, 2001.

Apituley, A., Pedergnana, M., Sneep, M., Pepijn, J., Loyola, D., Landgraf, J. and Borsdorff, T.: Sentinel-5 precursor/TROPOMI Level 2 Product User Manual Carbon Monoxide document number : SRON-S5P-LEV2-MA-002, : https://sentinels.copernicus.eu/documents/247904/2474726/Sentinel-5P-Level-2-Product-User-Manual-Carbon-Monoxide, 2018.

Bieser, J., Aulinger, A., Matthias, V., Quante, M. and Denier Van Der Gon, H. A. C.: Vertical emission profiles for Europe based on plume rise calculations, Environmental Pollution, https://doi.org/10.1016/j.envpol.2011.04.030, 2011.

Boersma, K. F., Eskes, H. J. and Brinksma, E. J.: Error analysis for tropospheric NO2 retrieval from space, Journal of Geo physical Research Atmospheres, 109, D04311,https://doi:10.1029/2003jd003962, 2004.

Boersma, K. F., Eskes, H. J., Dirksen, R. J., Van Der A, R. J., Veefkind, J. P., Stammes, P., Huijnen, V., Kleipool, Q. L., Sneep, M., Claas, J., Leitão, J., Richter, A., Zhou, Y. and Brunner, D.: An improved tropospheric NO2 column retrieval algorithm for the Ozone Monitoring Instrument, Atmospheric Measurement Techniques, 4(9), 1905–1928, https://doi.org/10.5194/amt-4-1905-2011, 2011.

Boersma, K. F., Vinken, G. C. M. and Eskes, H. J.: Representativeness errors in comparing chemistry transport and chemistry climate models with satellite UV-Vis tropospheric column retrievals, Geoscienctific Model Development, 9(2), 875–898, https://doi.org/10.5194/gmd-9-875-2016, 2016.

Boersma, K. F., Eskes, H. J., Richter, A., De Smedt, I., Lorente, A., Beirle, S., Van Geffen, J. H. G. M., Zara, M., Peters, E., Van Roozendael, M., Wagner, T., Maasakkers, J. D., Van Der A, R. J., Nightingale, J., De Rudder, A., Irie, H., Pinardi, G., Lambert, J. C. and Compernolle, S. C.: Improving algorithms and uncertainty estimates for satellite NO2 retrievals: Results from the quality assurance for the essential climate variables (QA4ECV) project, Atmospheric Measurement Techniques, 11(12), 6651–6678, https://doi.org/10.5194/amt-11-6651-2018, 2018.

Borsdorff, T., Hasekamp, O. P., Wassmann, A. and Landgraf, J.: Insights into Tikhonov regularization: Application to trace gas column retrieval and the efficient calculation of total column averaging kernels, Atmospheric Measurement Techniques , 7(2), 523–535, https://doi.org/10.5194/amt-7-523-2014, 2014.

Borsdorff, T., Andrasec, J., De Brugh, J. A., Hu, H., Aben, I. and Landgraf, J.: Detection of carbon monoxide pollution from cities and wildfires on regional and urban scales: the benefit of CO column retrievals from SCIAMACHY 2.3 μm measurements under cloudy conditions, Atmospheric Measurement Techniques , 11(5), 2553–2565, https://doi.org/10.5194/amt-11-2553-2018, 2018a.

Borsdorff, T., Aan de Brugh, J., Hu, H., Aben, I., Hasekamp, O. and Landgraf, J.: Measuring Carbon Monoxide With TROPOMI: First Results and a Comparison With ECMWF-IFS Analysis Data, Geophysical Research. Letter , 45(6), 2826–2832, https://doi.org/10.1002/2018GL077045, 2018b.

Borsdorff, T., Aan De Brugh, J., Hu, H., Hasekamp, O., Sussmann, R., Rettinger, M., Hase, F., Gross, J., Schneider, M., Garcia, O., Stremme, W., Grutter, M., Feist, Di. G., Arnold, S. G., De Mazière, M., Kumar Sha, M., Pollard, D. F., Kiel, M., Roehl, C., Wennberg, P. O., Toon, G. C. and Landgraf, J.: Mapping carbon monoxide pollution from space down to city scales with daily global coverage, Atmospheric Measurement Techniques , 11(10), 5507–5518, https://doi.org/10.5194/amt-11-5507-2018, 2018c.

Bovensmann, H., Burrows, J. P., Buchwitz, M., Frerick, J., Noël, S., Rozanov, V. V., Chance, K. V. and Goede, A. P. H.: SCIAMACHY: Mission objectives and measurement modes, Journal of the Atmospheric Sciences, https://doi.org/10.1175/1520-0469(1999)056<0127:SMOAMM>2.0.CO;2, 1999.

Browne, E. C., Min, K. E., Wooldridge, P. J., Apel, E., Blake, D. R., Brune, W. H., Cantrell, C. A., Cubison, M. J., Diskin, G. S., Jimenez, J. L., Weinheimer, A. J., Wennberg, P. O., Wisthaler, A. and Cohen, R. C.: Observations of total RONO2 over the boreal forest: NO x sinks and HNO3 sources, Atmospheric Chemistry and Physics, https://doi.org/10.5194/acp-13-4543-2013, 2013.

Burkholder, J. B., Sander, S. P., Abbatt, J. P. D., Barker, J. R., Huie, R. E., Kolb, C. E., Kurylo, M. J., Orkin, V. L., Wilmouth, D. M. and Wine, P. H.: JPL Publication 15-10 Chemical Kinetics and Photochemical Data for Use in Atmospheric Studies, , (18) : https://jpldataeval.jpl.nasa.gov/, 2015.

Castellanos, P. and Boersma, K. F.: Reductions in nitrogen oxides over Europe driven by environmental policy and economic recession, Scientific Reports , 2(2), 1–7, https://doi.org/10.1038/srep00265, 2012.

Crippa, M., Janssens-Maenhout, G., Dentener, F., Guizzardi, D., Sindelarova, K., Muntean, M., Van Dingenen, R. and Granier, C.: Forty years of improvements in European air quality: Regional policy-industry interactions with global impacts, Atmospheric Chemistry and Physics, https:// https://doi.org/10.5194/acp-16-3825-2016, 2016.

de Gouw, J. A., Parrish, D. D., Brown, S. S., Edwards, P., Gilman, J. B., Graus, M., Hanisco, T. F., Kaiser, J., Keutsch, F. N., Kim, S.-W., Lerner, B. M., Neuman, J. A., Nowak, J. B., Pollack, I. B., Roberts, J. M., Ryerson, T. B., Veres, P. R., Warneke, C., and Wolfe, G. M.: Hydrocarbon Removal in Power Plant Plumes Shows Nitrogen Oxide Dependence of Hydroxyl Radicals. Geophysical Research Letters, 0–2. https://doi.org/10.1029/2019GL083044, 2019

Dekker, I. N., Houweling, S., Aben, I., Röckmann, T., Krol, M., Martínez-Alonso, S., Deeter, M. N. and Worden, H. M.: Quantification of CO emissions from the city of madrid using MOPITT satellite retrievals and WRF simulations, Atmospheric Chemistry and Physics , 17(23), 14675–14694, https://doi.org/10.5194/acp-17-14675-2017, 2017.

Eskes, H.J., van Geffen, J., Boersma, K.F., Eichmann, K.-U, Apituley, A., Pedergnana, M., Sneep, M., Pepijn, J., Loyola, D.: Level 2 Product User Manual Henk Eskes, S5P-KNMI-L2-0021-MA, issue 3.0.0, 27 March 2019, https://earth.esa.int/documents/247904/2474726/Sentinel-5P-Level-2-Product-User-Manual-Nitrogen-Dioxide, 2019

Eskes, H. J. and Boersma, K. F.: Averaging kernels for DOAS total-column satellite retrievals, Atmospheric Chemistry and Physics ., 3(5), 1285–1291, https://doi.org/10.5194/acp-3-1285-2003, 2003.

Eskes, H. J. and Eichmann, K.-U.: S5P Mission Performance Centre Nitrogen Dioxide [L2__NO2___] Readme, Esa https://sentinel.esa.int/documents/247904/3541451/Sentinel-5P-Nitrogen-Dioxide-Level-2-Product-Readme-File, 2019.

Farmer, D. K., Perring, A. E., Wooldridge, P. J., Blake, D. R., Baker, A., Meinardi, S., Huey, L. G., Tanner, D., Vargas, O. and Cohen, R. C.: Impact of organic nitrates on urban ozone production, Atmospheric Chemistry and Physics. https://doi.org/10.5194/acp-11-4085-2011.

Flagan, R. C. and Seinfeld, J. H.: Fundamentals of Air Pollution Engineering., Prentice-Hall, Inc., Englewood CLiffs, NJ. ISBN 0-13-332537-7. http://resolver.caltech.edu/CaltechBOOK:1988.001, 1988.

Frey, H. C. and Zheng, J.: Quantification of variability and uncertainty in air pollutant emission inventories: Method and case study for utility NOx emissions, Journal of the Air Waste Manag. Association, 52(9), 1083–1095, https://doi.org/10.1080/10473289.2002.10470837, 2002.

Granier, C., Bessagnet, B., Bond, T., D'Angiola, A., van der Gon, H. D., Frost, G. J., Heil, A., Kaiser, J. W., Kinne, S., Klimont, Z., Kloster, S., Lamarque, J. F., Liousse, C., Masui, T., Meleux, F., Mieville, A., Ohara, T., Raut, J. C., Riahi, K., Schultz, M. G., Smith, S. J., Thompson, A., van Aardenne, J., van der Werf, G. R. and van Vuuren, D. P.: Evolution of anthropogenic and biomass burning emissions of air pollutants at global and regional scales during the 1980-2010 period, Climatic Change, 109(1), 163–190 https://doi.org/:10.1007/s10584-011-0154-1, 2011.

Griffin, D., Zhao, X., McLinden, C. A., Boersma, F., Bourassa, A., Dammers, E., Degenstein, D., Eskes, H., Fehr, L. Fioletov, V., Hayden, K., Kharol, S. K., Li, S. M., Makar, P., Martin, R. V., Mihele, C., Mittermeier, R. L., Krotkov, N., Sneep, M., Lamsal, L. N., Linden, M. ter, Geffen, J. van, Veefkind, P. and Wolde, M.: High-Resolution Mapping of Nitrogen Dioxide With TROPOMI: First Results and Validation Over the Canadian Oil Sands, Geophysical Research Letters, https://doi.org/10.1029/2018GL081095 , 2019.

Guerreiro, C. B. B., Foltescu, V. and de Leeuw, F.: Air quality status and trends in Europe, Atmospheric Environment, 98, 376–384, https://doi.org/10.1016/j.atmosenv.2014.09.017, 2014.

Hakkarainen, J., Ialongo, I. and Tamminen, J.:Direct space-based observations of anthropogenic CO 2 emission areas from OCO-2, Geophysical Research. Letter, 43, 11, 400– 11,406, https://doi.org/10.1002/2016GL070885.,2015.

Huijnen, V., Pozzer, A., Arteta, J., Brasseur, G., Bouarar, I., Chabrillat, S., Christophe, Y., Doumbia, T., Flemming, J., Guth, J., Josse, B., Karydis, V. A., Marécal, V. and Pelletier, S.: Quantifying uncertainties due to chemistry modelling - Evaluation of tropospheric composition simulations in the CAMS model (cycle 43R1), Geoscientific Model Development,., 12(4), 1725–1752, https://doi.org/10.5194/gmd-12-1725-2019, 2019.

Jacob, D. J.: Introduction to Atmospheric Chemistry: Daniel J. Jacob; Princeton University Press, Princeton, NJ, 1999, 266pp., ISBN 0-691-00185-5, Atmospheric Environment. https://doi.org/10.1016/s1352-2310(00)00432-5, 1999.

Janssens-Maenhout, G., Crippa, M., Guizzardi, D., Dentener, F., Muntean, M., Pouliot, G., Keating, T., Zhang, Q., Kurokawa, J., Wankmüller, R., Denier Van Der Gon, H., Kuenen, J. J. P., Klimont, Z., Frost, G., Darras, S., Koffi, B. and Li, M.: HTAP-v2.2: A mosaic of regional and global emission grid maps for 2008 and 2010 to study hemispheric transport of air pollution, Atmospheric Chemistry and Physics,, 15(19), 11411–11432, https://doi.org/10.5194/acp-15-11411-2015, 2015.

Jiang, Z., Worden, J. R., Worden, H., Deeter, M., Jones, D. B. A., Arellano, A. F. and Henze, D. K.: A 15-year record of CO emissions constrained by MOPITT CO observations, Atmospheric Chemistry and Physics, 17(7), 4565–4583.

https://doi.org/10.5194/acp-17-4565-2017, 2017.

Konovalov, I. B., Berezin, E. V., Ciais, P., Broquet, G., Beekmann, M., Hadji-Lazaro, J., Clerbaux, C., Andreae, M. O., Kaiser, J. W. and Schulze, E. D.: Constraining CO 2 emissions from open biomass burning by satellite observations of co-emitted species: A method and its application to wildfires in Siberia, Atmospheric Chemistry and Physics. https://doi.org/0.5194/acp-14-10383-2014, 2014.

Korontzi, S., Ward, D. E., Susott, R. A., Yokelson, R. J., Justice, C. O., Hobbs, P. V., Smithwick, E. A. H. and Hao, W. M.: Seasonal variation and ecosystem dependence of emission factors for selected trace gases and PM 2.5 for southern African savanna fires , Journal of Geophysical Research: Atmospheres, 108(D24), 4758. https://doi.org/10.1029/2003jd003730, 2003.

Krol, M., Houweling, S., Bregman, B., Broek, M. Van Den, Segers, A., Velthoven, P. Van, Peters, W. and Dentener, F.: and Physics The two-way nested global chemistry-transport zoom model TM5 : algorithm and applications, Atmospheric Chemistry and Physics, 417–432, https://doi.org/10.5194/acp-5-417-2005, 2005.

Lambert, J.-C., A. Keppens, D. Hubert, B. Langerock, K.-U. Eichmann, Q. Kleipool, M. Sneep, T. Verhoelst, T. Wagner, M. Weber, C. Ahn, A. Argyrouli, D. Balis, K.L. Chan, S. Compernolle, I. De Smedt, H. Eskes, A.M. Fjæraa, K. Garane, J.F. Gleason, F. Gouta, and P. W.: Sentinel-5 Precursor Mission Performance Centre Quarterly Validation Report of the Copernicus Sentinel-5 Precursor Operational Data Products # 03 : July 2018 – May 2019, 1–125, 2019.

Landgraf, J., Brugh, J. De, Scheepmaker, R. A., Borsdorff, T., Houweling, S. and Hasekamp, O. P.: Algorithm Theoretical Baseline Document for Sentinel-5 Precursor : Carbon Monoxide Total Column Retrieval J . Pepijn Veefkind, 2016a.

Landgraf, J., Aan De Brugh, J., Scheepmaker, R., Borsdorff, T., Hu, H., Houweling, S., Butz, A., Aben, I. and Hasekamp, O.: Carbon monoxide total column retrievals from TROPOMI shortwave infrared measurements, Atmospheric Measurement Techniques, 9(10), 4955–4975. https://doi.org/10.5194/amt-9-4955-2016b.

Lang, M. N., Gohm, A. and Wagner, J. S.: The impact of embedded valleys on daytime pollution transport over a mountain range, Atmospheric Chemistry and Physics. 15, 11981–11998, https://doi.org/:10.5194/acp-15-11981-2015, 2015.

Lorente, A., Folkert Boersma, K., Yu, H., Dörner, S., Hilboll, A., Richter, A., Liu, M., Lamsal, L. N., Barkley, M., De Smedt, I., Van Roozendael, M., Wang, Y., Wagner, T., Beirle, S., Lin, J. T., Krotkov, N., Stammes, P., Wang, P., Eskes, H. J. and Krol, M.: Structural uncertainty in air mass factor calculation for NO2 and HCHO satellite retrievals, Atmospheric Measurement Techniques, 10(3), 759–782. https://doi.org/10.5194/amt-10-759-2017.

Ma, J. and van Aardenne, J. A.: Impact of different emission inventories on simulated tropospheric ozone over China: a regional chemical transport model evaluation, Atmospheric Chemistry and Physics. 4, 877–887, https://doi.org/10.5194/acp-4-877-2004, 2004.

Mijling, B. and Van Der A, R. J.: Using daily satellite observations to estimate emissions of short-lived air pollutants on a mesoscopic scale, Journal of Geophysical Research Atmospheres, *117*(17), 1–20. https://doi.org/10.1029/2012JD017817, 2012.

Miyazaki, K., Eskes, H., Sudo, K., Folkert Boersma, K., Bowman, K. and Kanaya, Y.: Decadal changes in global surface NOx emissions from multi-constituent satellite data assimilation, Atmospheric Chemistry and Physics, 17(2), 807–837,

https://doi.org/10.5194/acp-17-807-2017, 2017.

Pommier, M., McLinden, C. A. and Deeter, M.: Relative changes in CO emissions over megacities based on observations from space, Geophysical Research Lettter, 40(14), 3766–3771,https:// doi.org/10.1002/grl.50704, 2013.

Reuter, M., Buchwitz, M., Hilboll, A., Richter, A., Schneising, O., Hilker, M., Heymann, J., Bovensmann, H. and Burrows, J. P.: Decreasing emissions of NOx relative to CO2 in East Asia inferred from satellite observations, Nature Geoscience, 7(11), 792–795, https://doi.org/10.1038/ngeo2257, 2014.

Reuter, M., Buchwitz, M., Schneising, O., Krautwurst, S., O'Dell, C. W., Richter, A., Bovensmann, H. and Burrows, J. P.: Towards monitoring localized CO2 emissions from space: co-located regional CO and NO2 enhancements observed by the OCO-2 and S5P satellites, Atmospheric Chemistry and Physics Discussions, (2), 1–19, https://doi.org/10.5194/acp-2019-15, 2019, 2019.

Romer, P. S., Duffey, K. C., Wooldridge, P. J., Edgerton, E., Baumann, K., Feiner, P. A., Miller, D. O., Brune, W. H., Koss, A. R., De Gouw, J. A., Misztal, P. K., Goldstein, A. H. and Cohen, R. C.: Effects of temperature-dependent NOx emissions on continental ozone production, Atmospheric Chemistry and Physics. https://doi.org/10.5194/acp-18-2601-2018, 2018.

Romer Present, P. S., Zare, A. and Cohen, R. C.: The changing role of organic nitrates in the removal and transport of NOx, Atmospheric Chemistry and Physics Discussions, *x*, 1–18. https://doi.org/0.5194/acp-2019-471, 2019.

Schneider, P., Lahoz, W. A. and Van Der A, R.: Recent satellite-based trends of tropospheric nitrogen dioxide over large urban agglomerations worldwide, Atmospheric Chemistry and Physics, 15(3), 1205–1220. https://doi.org/10.5194/acp-15-1205-2015.

Seinfeld, J. H. and Pandis, S. N.: Atmospheric Chemistry and Physics: From Air Pollution to Climate Change SECOND EDITION., John Wiley and Sons Inc., 2006.

Silva, S. and Arellano, A.: Characterizing Regional-Scale Combustion Using Satellite Retrievals of CO, NO2 and CO2, Remote Sensing , 9(7), 744, https://doi.org/10.3390/rs9070744, 2017.

Silva, S. J., Arellano, A. F. and Worden, H. M.: Toward anthropogenic combustion emission constraints from space-based analysis of urban CO2/CO sensitivity, Geophysical Research Letters, 40(18), 4971–4976,https://doi.org/ 10.1002/grl.50954, 2013.

Sinha, P., Hobbs, P. V., Yokelson, R. J., Bertschi, I. T., Blake, D. R., Simpson, I. J., Gao, S., Kirchstetter, T. W. and Novakov, T.: Emissions of trace gases and particles from savanna fires in southern Africa, Journal of Geophysical Research: Atmospheres. https://doi:10.1029/2002JD002325, 2003.

Sobanski, N., Thieser, J., Schuladen, J., Sauvage, C., Song, W., Williams, J., Lelieveld, J. and Crowley, J. N.: Day and night-time formation of organic nitrates at a forested mountain site in south-west Germany, Atmospheric Chemistry and Physics. https://doi.org/10.5194/acp-17-4115-2017.

Tang, W. and Arellano, A. F.: Investigating dominant characteristics of fires across the Amazon during 2005-2014 through satellite data synthesis of combustion signatures, Journal of Geophysical Research: Atmospheres. https://doi.org/10.1002/2016jd025216, 2017.

Tang, W., Arellano, A. F., Gaubert, B., Miyazaki, K. and Worden, H. M.: Satellite data reveal a common combustion emission pathway for major cities in China, Atmospheric Chemistry and Physics. https://doi.org/10.5194/acp-19-4269-2019.

United Nations: World Urbanization Prospects In Demographic Research (Vol 12). https://doi.org/10.4054/demres.2005.12.9 , 2018.

Vallero, D. A.: Fundamentals of Air Pollution, In Fundamentals of Air Pollution. Elsevier Inc. https://doi.org/10.1016/B978-0-12-373615-4.X5000-6, 2007.

van Geffen, J. H. G. M., Eskes, H. J., Boersma, K. F., Maasakkers, J. D. and Veefkind, J. P.: TROPOMI ATBD of the total and tropospheric NO2 data products, S5P-KNMI-L2-0005-RP, issue 1.4.0, 6 Feburary 2019, S5P-Knmi-L2-0005-Rp, (1.4.0), 1–76 https://sentinel.esa.int/documents/247904/2476257/Sentinel-5P-TROPOMI-ATBD-NO2-data-products, 2019.

Veefkind, J. P., Aben, I., McMullan, K., Förster, H., de Vries, J., Otter, G., Claas, J., Eskes, H. J., de Haan, J. F., Kleipool, Q., van Weele, M., Hasekamp, O., Hoogeveen, R., Landgraf, J., Snel, R., Tol, P., Ingmann, P., Voors, R., Kruizinga, B., Vink, R., Visser, H. and Levelt, P. F.: TROPOMI on the ESA Sentinel-5 Precursor: A GMES mission for global observations of the atmospheric composition for climate, air quality and ozone layer applications, Remote Sensing of Environment, https:// doi.org/10.1016/j.rse.2011.09.027, 2012.

Ward, D. E., Hao, W. M., Susott, R. A., Babbitt, R. E., Shea, R. W., Kauffman, J. B. and Justice, C. O.: Effect of fuel composition on combustion efficiency and emission factors for African savanna ecosystems, Journal of Geophysical Research : Atmospheres. https://, doi.org/10.1029/95jd02595, 1996.

Williams, J. E., Folkert Boersma, K., Le Sager, P. and Verstraeten, W. W.: The high-resolution version of TM5-MP for optimized satellite retrievals: Description and validation, Geoscientific Model Development, 10(2), 721–750. https://doi.org/10.5194/gmd-10-721-2017, 2017 .

Yokelson, R. J., Griffith, D. W. T. and Ward, D. E.: Open-path Fourier transform infrared studies of large-scale laboratory biomass fires, Journal of Geophysical Research: Atmospheres, *101*(D15), 21067–21080. https://doi.org/10.1029/96jd01800 1996.

Yokelson, R. J., Bertschi, I. T., Christian, T. J., Hobbs, P. V., Ward, D. E. and Hao, W. M.: Trace gas measurements in nascent, aged, and cloud-processed smoke from African savanna fires by airborne Fourier transform infrared spectroscopy (AFTIR), Journal of Geophysical Research: Atmospheres. https://doi.org/10.1029/2002jd002322, 2003.

Zhao, Y., Nielsen, C. P., Lei, Y., McElroy, M. B. and Hao, J.: Quantifying the uncertainties of a bottom-up emission inventory of anthropogenic atmospheric pollutants in China, Atmospheric Chemistry and Physics. https://doi.org/10.5194/acp-11-2295-2011, 2011.

Zhao, Y., Nielsen, C. P., McElroy, M. B., Zhang, L. and Zhang, J.: CO emissions in China: Uncertainties and implications of improved energy efficiency and emission control,AtmosphericEnvironment.https://doi.org/10.1016/j.atmosenv.2011.12.015, 2012.

Appendix A

Derivation of Eq. (6)

For CO:

The mass balance equation for CO is

$$\frac{d\Delta XCO}{dt} = Emission - loss\ by\ transport$$

$$\frac{d\Delta XCO}{dt} = E_{CO} - \frac{U}{lx}\Delta XCO$$

In steady state $\frac{d\Delta X_{CO}}{dt}$ is zero.

$$E_{CO} = \frac{U}{lx}\Delta XCO$$

where, ΔXCO is the enhancement of CO in the city in ppb, U is the wind speed in ms^{-1} , lx is the diameter of the city in meter (m).

For NO_2:

The mass balance equation for NO_2 is:

$$\frac{d\Delta XNO_2}{dt} = Emission - loss\ by\ the\ transport - chemical\ loss$$

$$\frac{d\Delta XNO_2}{dt} = E_{NO_2} - \frac{U}{lx}\Delta XNO_2 - \frac{\Delta XNO_2}{\tau}$$

In the steady state, $\frac{d\Delta X_{NO2}}{dt}$ is zero and τ is $\frac{1}{K[OH]}$, K is the rate constant reaction of NO_2 with OH, $2.8e^{-11}\left(\frac{T}{300}\right)^{-1.3}$ cm^3 $molecules^{-1}second^{-1}$ (Burkholder et al., 2015), T in kelvin and OH (molecules cm^{-3}) is the average boundary layer concentration.

$$E_{NO_2} = \Delta XNO_2\left(\frac{U}{w} + \frac{1}{\frac{1}{K[OH]}}\right)$$

where, ΔXNO_2 is the enhancement of NO_2 in the City in ppb, U is the wind speed in ms^{-1}, lx is the diameter of the city in meter(m).

Ratio:

$$\frac{E_{NO_2}}{E_{CO}} = \frac{\Delta XNO_2}{\Delta XCO}.\left(\frac{\frac{U}{lx} + K[OH]}{\frac{U}{lx}}\right)$$

Influence of averaging kernel:

$$\frac{E_{NO2}}{E_{CO}} = \frac{\Delta XNO_2}{\Delta XCO} \frac{\left(\frac{U}{lx} + K[OH]\right)}{\frac{U}{lx}} . \frac{1}{(1 - A_{influence})}$$

Where, $A_{influence}$ is the influence of the averaging kernel on $\Delta XNO_2/\Delta XCO$

Appendix B

Derivation of Tropospheric Averaging kernel (A) for NO_2 as described by Eskes et al., (2018)

$$A_{trop} = \left(\frac{M}{M_{trop}}\right) * A_{total} \quad \left(l \leq l_{tp}^{TM5}\right)$$

$$A_{trop} = 0, \quad \left(l > l_{tp}^{TM5}\right)$$

where, M is the total mass factor and M_{trop} is the air mass factor for the troposphere, l_{tp}^{TM5} is the TM5 tropopause layer index.

Appendix C

$$Without\ A = \frac{\Delta NO_{2_{CAMS}}}{\Delta CO_{CAMS}}$$

$$NO2_{new\ CAMS} = NO_{2_{CAMS}} * A_{No2\ TROPOMI}$$

$$CO_{new\ CAMS} = CO_{CAMS} * A_{CO\ TROPOMI}$$

$$With\ A = \frac{\Delta NO_{2_{new\ CAMS}}}{\Delta CO_{new\ CAMS}}$$

$$A_{influence} = \frac{(Without\ A - with\ A)}{Without\ A} . 100\%$$

where, $NO_{2_{CAMS}}$ and CO_{CAMS} is the CAMS column densities derived for NO2 and CO whereas $\Delta NO_{2_{CAMS}}$ and ΔCO_{CAMS} is the city enhancement of NO_2 and CO. $A_{No2\ TROPOMI}$ and $A_{CO\ TROPOMI}$ is the TROPOMI averaging kernel for NO_2 and CO.